NANO LETTERS

pubs.acs.org/NanoLett Letter

Edge-Topological Regulation for *in Situ* Fabrication of Bridging Nanosensors

Jiangyang Liu, Hao Zeng, Guozhu Zhang, Wenjun Li, Kazuki Nagashima, Tsunaki Takahashi, Takuro Hosomi, Wataru Tanaka, Masaki Kanai, and Takeshi Yanagida*

Cite This: *Nano Lett.* 2022, 22, 2569−2577 Read Online

ACCESS | Metrics & More | Article Recommendations | Supporting Information

ABSTRACT: *In situ* fabrication of well-defined bridging nanostructures is an interesting and unique approach to three-dimensionally design nanosensor structures, which are hardly attainable by other methods. Here, we demonstrate the significant effect of edge-topological regulation on *in situ* fabrication of ZnO bridging nanosensors. When employing seed layers with a sharp edge, which is a well-defined structure in conventional lithography, the bridging angles and electrical resistances between two opposing electrodes were randomly distributed. The stochastic nature of bridging growth direction at the sharp edges inherently causes such unintentional variation of structural and electrical properties. We propose an edgeless seed layer structure using a two-layers resist method to solve the above uncontrollability of bridging nanosensors. Such bridging nanosensors not only substantially improved the uniformity of structural and electrical properties between two opposing electrodes but also significantly enhanced the sensing responses for NO_2 with the smaller variance and the lower limit of detection via *in situ* controlled electrical contacts.

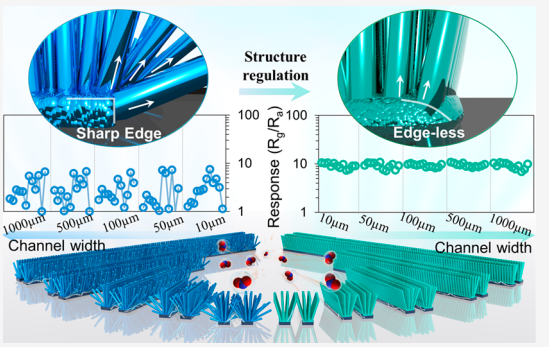

KEYWORDS: *In situ fabrication, Bridging nanostructure, Edge-topological regulation, Hydrothermal growth, Nanosensor*

INTRODUCTION

Manipulating and tailoring three-dimensional (3D) nanostructures using *in situ* fabrication of bottom−up methods is one of major goals in nanotechnology.[1−5] Such well-defined 3D nanostructures are promising candidates as novel sensor structures, which had not been fabricable by conventional methodologies.[6−10] The *in situ* fabrication technique is particularly interesting to define the spatial location of nanosensors on a patterned substrate with the resolution of current lithographic technology.[11−13] This fruitful combination of top−down lithographic technology and bottom−up crystal growth technology in *in situ* fabrication of nanosensors offers an important foundation to construct highly integrated nanosensors via advanced semiconductor technologies.[14−16] Among various 3D nanosensors, a bridging nanostructure between two opposing electrodes is a promising sensor structure because a contact point between two nanostructures plays an essential role in sensing characteristics of various gases.[17−20] To the best of our knowledge, such *in situ* fabrication of bridging nanosensors was first demonstrated by Qi and Dai et al. using carbon nanotubes for NH_3 and NO_2 sensing.[21] This *in situ* fabrication of bridging nanosensors has been successfully applied to various sensor materials, e.g., Si nanowire bridging nanosensors[22] for HCl and NH_3, ZnO bridging nanosensors[23,24] for NO_2 [23] or H_2S,[24] SnO_2 nanowire bridging nanosensors for liquefied petroleum gas and NH_3,[25] CuO nanowire bridging nanosensors of for CO,[26] and compound semiconductors GaN [27] or InAs [28] nanowire bridging nanosensors for NO_2 sensing. Although these studies consistently revealed that *in situ* fabrication of bridging nanosensors is a powerful approach to design three-dimensionally bridging nanosensors for various sensing materials, controlling precisely the structural and electrical properties of bridging nanostructures during *in situ* fabrication is still a challenging issue. Such uncontrollability will cause severe problems when constructing highly integrated nanosensors with high reliability, spatial uniformity, and reproducibility required for nanoelectronics.

This study reports the impact of edge-topological regulation on *in situ* fabrication of ZnO bridging nanostructures. The edge-geometry of seed structures for *in situ* fabrication critically determines the variability of the structural and electrical properties between two opposing electrodes via the stochastic nature of bridging growth direction at the sharp edges. Newly fabricated bridging nanosensors with edge-topological regu-

Received: November 29, 2021
Revised: February 7, 2022
Published: February 28, 2022

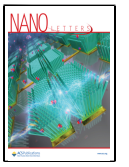

https://doi.org/10.1021/acs.nanolett.1c04600
Nano Lett. 2022, 22, 2569−2577

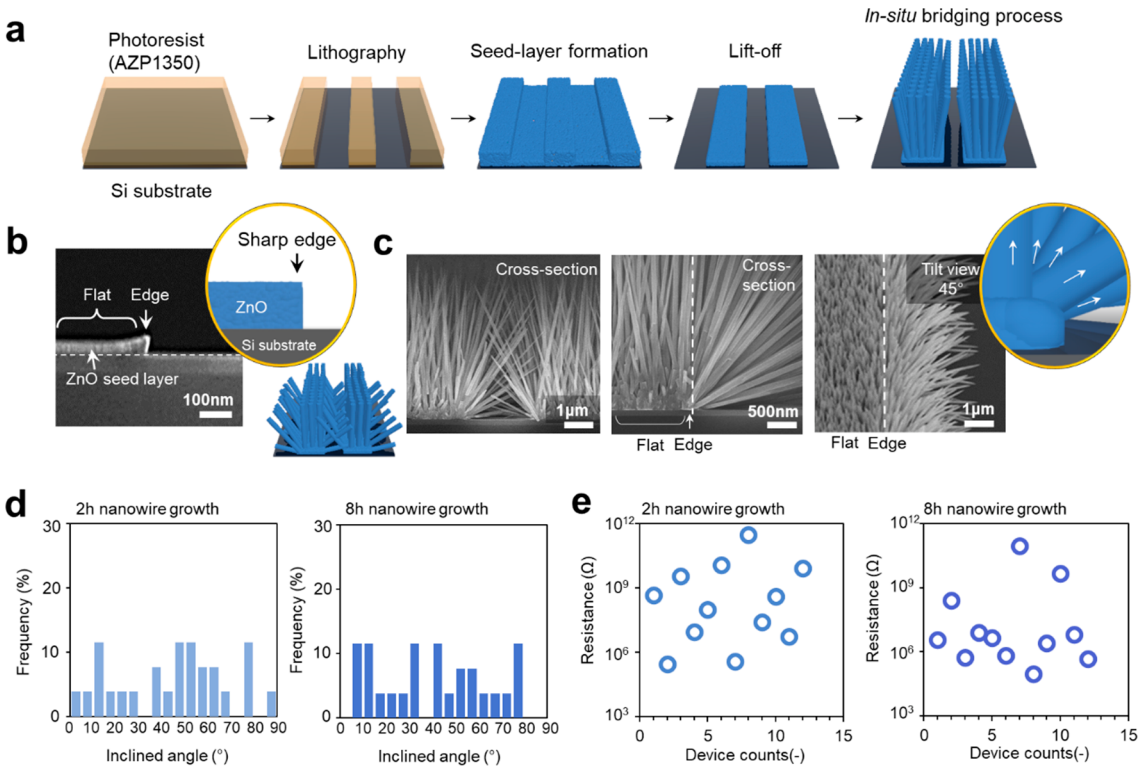

Figure 1. Bridging nanosensors fabricated from a sharp edge seed layer, and their structural and electrical properties: (a) schematic of experimental procedure to fabricate bridging nanosensors using conventional lift-off process; (b) cross-sectional scanning electron microscopy (SEM) image of fabricated seed layer with the well-defined sharp edge; (c) cross-sectional and tilted top-view (45°) SEM images of fabricated bridging ZnO nanowires at edge and flat area of seed layer; (d) bridging angle distribution between two opposing seed layers (2 and 8 h nanowire growth); (e) statistical variation of electrical resistances of fabricated nanosensors (2 and 8 h nanowire growth).

lations exhibited much superior well-controlled structural, electrical, and gas sensing properties when compared with those using conventional shape edge seed structures.

RESULTS AND DISCUSSION

Figure 1a shows the experimental procedure to fabricate bridging nanosensors using lithographically defined ZnO seed layers on Pt electrodes. The conventional lithographic process is employed to define the patterns of electrodes and seed layers.[29,30] Bridging ZnO nanosensors are then *in situ* formed between two opposing seed layers on the substrate using hydrothermal crystal growth.[31−33] The length of ZnO nanowires can be controlled as a function of the growth time.[34,35] Figure 1b shows the cross-sectional scanning electron microscopy (SEM) image of a fabricated seed layer, showing the sharp edge defined by lithography. Figure 1c shows the SEM images of bridging nanosensors fabricated. As clearly seen in the SEM images, the fabricated ZnO nanowires were significantly inclined with respect to the vertical direction of the substrate. Figure 1c also shows the comparison between edges and flat planes of ZnO seed layers on the cross-sectional and tilted (45°) SEM images. Clearly, the inclined ZnO nanowires were preferentially formed only at edges of seed layers. Since it is well-known that the surface energies at edges are in general higher than those at flat planes due the increased number of surface dangling bonds, a nucleation during ZnO hydrothermal growths preferentially occurs at edges.[36−38] More importantly, the growth direction of ZnO nanowires at edges cannot be intentionally defined and depends on the stochastic event where a nucleation around edges occurs.[39,40]

The angle distribution of ZnO nanowires between two opposing seed layers was analyzed from the cross-sectional SEM images, with the data shown in Figure 1d. The random distribution of measured angle values can be seen. Data also revealed that the inclined ZnO nanowires emerged even in the early growth stage. This random angle distribution has been consistently observed for all bridging nanosensors fabricated from a sharp edge seed layer (Figure S1). This unintentional structural variation resulted in the gigantic variation of electrical resistances between two opposing electrodes, as shown in Figure 1e. The electrical variability is in the range of 6 orders of magnitude for 12 bridging nanosensors fabricated by the identical experimental procedures. Thus, these results highlight that sharp edge structures of seed layers, which have been regarded as well-defined structures in conventional lithography, are detrimental to defining *in situ* fabrication of bridging nanosensors and their structural and electrical properties.

Next, we aim to control the above unintentional statistical variability of structural and electrical properties in *in situ* fabricated bridging nanosensors. On the basis of the aforementioned edge-based mechanism for variability, we propose an edgeless seed layer structure to define the growth direction for *in situ* fabrication of bridging nanosensors. Figure 2a shows the experimental procedure using a two-layers resist method to form an edgeless seed layer structure. The different side etching rate between the two laminated resists creates an undercut structure on the substrate (Figure S2), which results in an edgeless seed layer formation via a diffusion to the shadow area during the ZnO sputtering process. In addition,

https://doi.org/10.1021/acs.nanolett.1c04600
Nano Lett. 2022, 22, 2569−2577

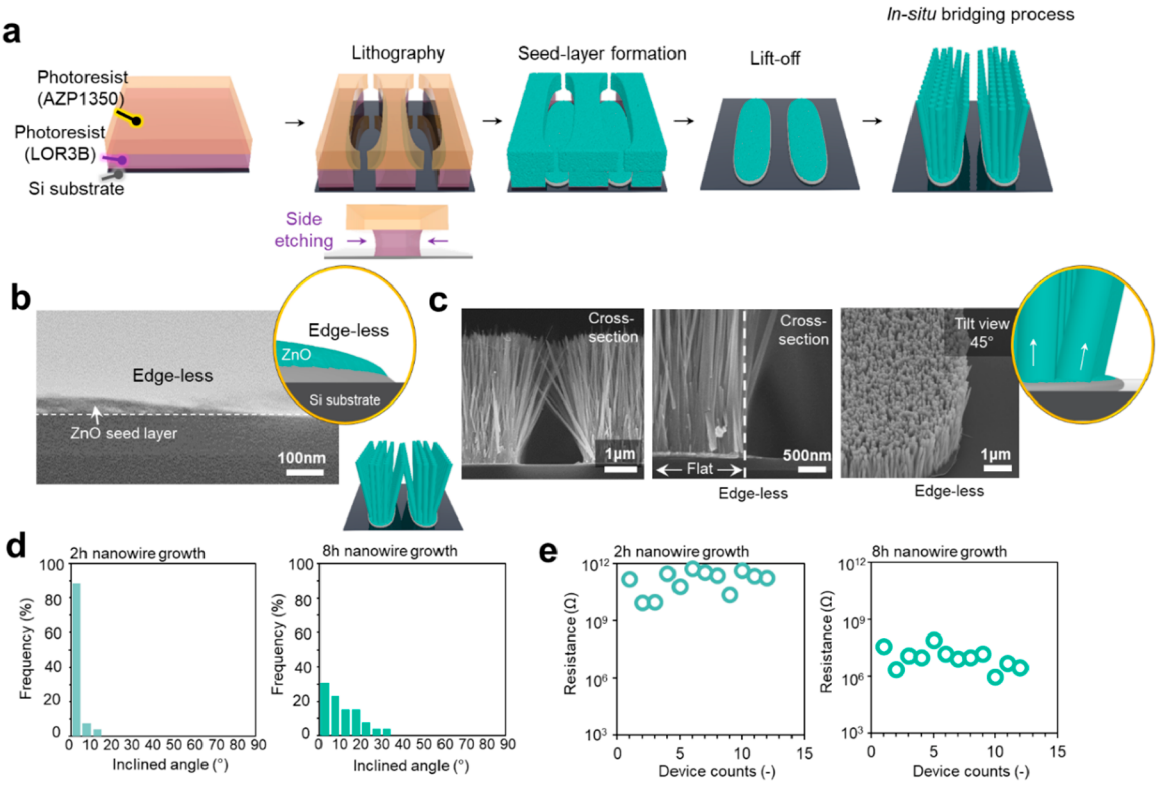

Figure 2. Bridging nanosensors fabricated from a newly proposed edgeless seed layer, and their structural and electrical properties: (a) schematic of experimental procedure to fabricate bridging nanosensors using conventional lift-off process; (b) cross-sectional SEM images of fabricated edgeless seed layer; (c) cross-sectional and tilted top-view (45°) SEM images of fabricated bridging ZnO nanowires at edge and flat area of seed layer; (d) angle distribution of ZnO nanowires between two opposing seed layers, where angles were calculated by inclined nanowire angle to vertical direction (2 and 8 h nanowire growth); (e) statistics of electrical resistances of fabricated nanosensors (2 and 8 h nanowire growth).

the top-view patterns of seed layers were designed to be rounded to avoid in-plane geometrical edges, since such in-edge structure also causes structural uncontrollability; see Figures S3−S6. The cross-sectional SEM image of fabricated edgeless seed layers shown in SEM image in Figure 2b revealed the absence of sharp edge structures in the seed layers. Figure 2c shows cross-sectional SEM images of fabricated bridging ZnO nanosensors using the above edgeless seed layers. Fabricated ZnO nanowires preferentially grow in the direction perpendicular to the substrate. Cross-sectional and tilted top-view (45°) SEM images for nanowires on edgeless ZnO seed layers were shown in Figure 2c, revealing that the edgeless seed layer enables defining of the growth angle of hydrothermal ZnO nanowires without unintentional inclined nanostructures. The same trend was confirmed for all bridging nanosensors fabricated from edgeless seed layers (Figure S7). Figure 2d shows the inclined angle distribution data, and Figure 2e shows the statistical distribution of electrical properties between two opposing electrodes for 12 bridging nanosensors. When comparing with Figure 1d and Figure 1e, there is a significant effect of edgeless seed layers on observed structural and electrical properties of bridging ZnO nanosensors. First, when compared with structures using sharp edge seed layers (Figure 1b), the ratio of inclined ZnO nanowires was substantially suppressed by using edgeless seed layers. As designed, the absence of edge structures in seed layers plays an essential role in observed improvements of directional controllability for *in situ* fabrication of bridging nanosensors. Second, such structural improvement substantially suppresses the unintentional statistical variability of electrical properties shown in Figure 2e. Thus, these results highlight that newly proposed methodology using edgeless seed layers allows us to perform well-defined *in situ* fabrication of bridging nanosensors without uncontrollable structural and electrical properties.

Figure 3 shows the effect of edge-topological regulation on NO_2 sensing response values. In order to examine the spatial uniformity of sensor characteristics, we systematically varied the width of bridging nanosensors from 10 to 1000 μm, as shown in the schematic and SEM images of Figure 3a. Figure 3b shows the effect of edge-topological regulation on the NO_2 sensing responses when varying the sensor channel width. The device geometries with the gap width of 2 μm and the nanowire length of ∼6 μm (8 h growth) were employed for NO_2 sensing performance at the operation temperature of 200 °C (Figures S8−S10). As clearly seen in the figures, the statistical variation of sensor responses strongly depends on the edge-topological regulation of bridging nanosensors. These statistical variance values were shown in the inset figures of Figure 3b. The statistical variance values of sensor responses for bridging nanosensors fabricated from sharp edge seed layers ranged from 2 to 6, much larger than those less than 1 for bridging nanosensors fabricated from edgeless seed layers. The difference between the two bridging nanosensors on the structural and electrical properties in Figure 1 and 2 well corresponds to the observed trends on the sensor responses and their statistical variations. In addition, for bridging nanosensors fabricated from edgeless seed layers, the sensor response value was almost constant when varying the width of sensors in the range of 10−1000 μm. This width insensitivity of sensor responses can be rigorously understood in terms of

https://doi.org/10.1021/acs.nanolett.1c04600
Nano Lett. 2022, 22, 2569−2577

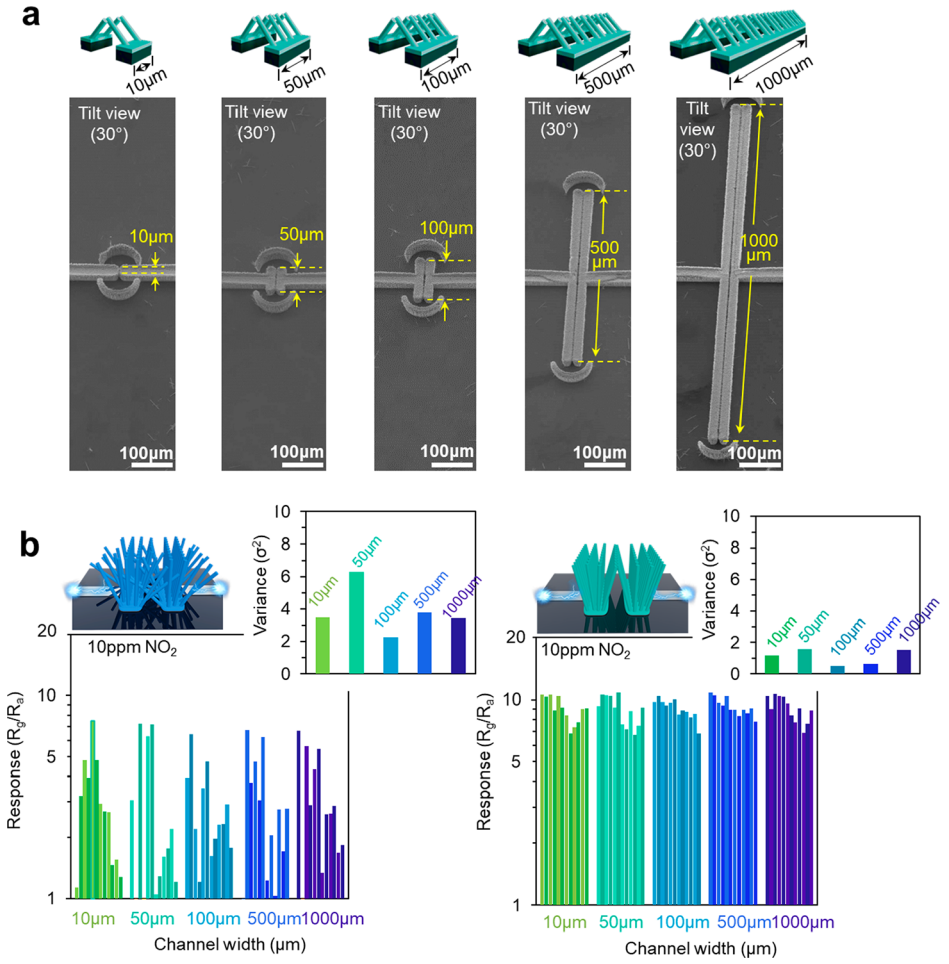

Figure 3. Effect of bridging structural difference on NO_2 sensing data of bridging nanosensors with widths ranging from 10 to 1000 μm: (a) schematic and SEM images of fabricated bridging nanosensors fabricated from the edgeless seed layer when varying the width from 10 to 1000 μm; (b) comparison between two bridging nanosensors fabricated from the sharp edge seed layer or the edgeless seed layer on NO_2 sensing response data, varying the width from 10 to 1000 μm, where the inset figures show the deviation value (σ^2) of bridging nanosensors.

the definition of sensor response R_g/R_a and their width, w, dependence. If the resistance changes with respect to sensor responses uniformly occur, both R_g and R_a are inversely proportional to w, explaining the width insensitivity of sensor responses as constant R_g/R_a. In addition to this width independent property of responses, the constant value of response regardless of sensor length L was also confirmed (Figure S11). These results highlight that the bridging nanosensors fabricated from edgeless seed layers are spatially uniform and highly scalable in the range of widths 10−1000 μm.

Next, we question how the sensing properties of bridging nanosensors correlate to their structural and electrical properties. To experimentally reveal this issue, we focus on the electrical contacts between two opposing electrodes. This is because most electrically resistive electrical contacts should be responsible for gas sensing characteristics. By utilization of *in situ* controllability of the present method, the electrical contacts can be systematically changed by varying the sensor gap size and the crystal growth time during the bridging process. Figure 4a shows the cross-sectional SEM images when varying the gap size when employing edgeless seed layers. There is an optimal growth time to complete the bridging process, which strongly depends on the device geometry-gap size. The wider gap sizes are, the longer is the growth time to accomplish bridging between two opposing electrodes. The results and details of fabricated devices are shown in Figure S12. Figure 4b shows the NO_2 (10 ppm) sensor responses when varying sensor gap size and the crystal growth time during bridging process. As clearly seen in the figure, there is a maximum of sensor responses as a function of nanowire length, which corresponds to the situation when the bridging process is optimized. Figure 4c shows the $I-V$ data for bridging nanosensors with various gap sizes (2−10 μm) when varying the nanowire lengths. Figure 4d shows the electrical resistance values extracted from $I-V$ curves under air and/or NO_2 (10 ppm) environments. As clearly seen, there are three distinct conditions of electrical contacts when varying the bridging growth time. For early stage 1, the bridging process does not complete, and thus the electrical resistance values are rather insulative around $10^9\Omega$ (GΩ level) without any sensing responses. For stage 2 when increasing the bridging growth time from stage 1, the electrical resistance values tend to decrease down to 10^5-10^6 Ω (MΩ level) with nonlinear $I-V$ data like double Schottky behaviors. For these electrical contacts, the NO_2 sensing responses are maximized for various gap-sized bridging nanosensors. When further increasing the bridging growth time, stage 3, the electrical resistance values also further decrease down to 10^3-10^4 Ω (kΩ level) with ohmic $I-V$ data. High-resolution cross-sectional SEM analysis

https://doi.org/10.1021/acs.nanolett.1c04600
Nano Lett. 2022, 22, 2569−2577

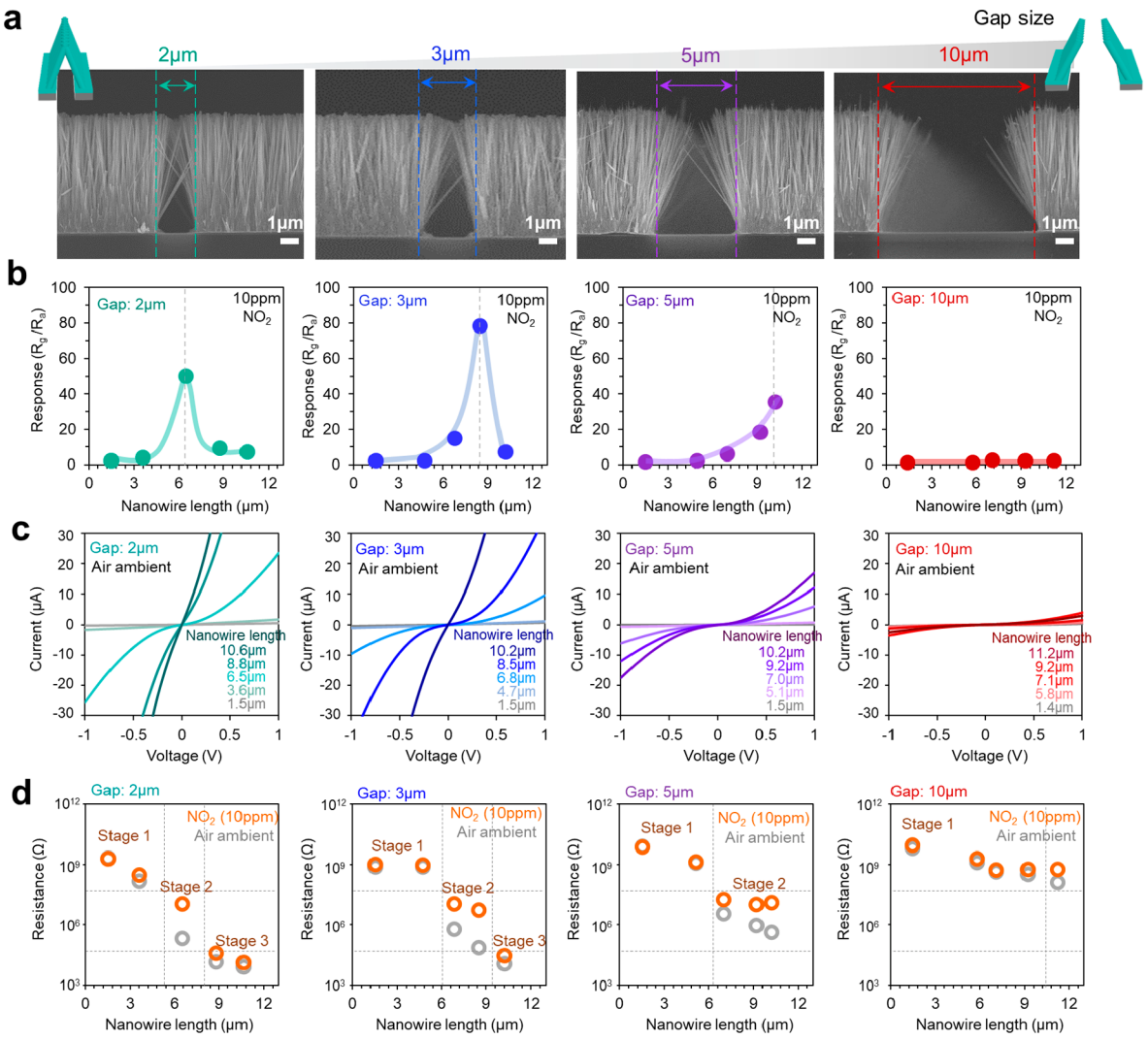

Figure 4. *In situ* structural controllability of bridging nanosensors using the proposed experimental procedure, and the *in situ* designability of NO_2 sensing characteristics: (a) cross-sectional SEM images of bridging nanosensors when varying the gap size from 2 to 10 μm; (b) correlation between NO_2 (10 ppm) sensor responses when varying sensor gap size and the nanowire length (evaluated from growth time); (c) $I-V$ data of bridging nanosensors when varying the gap sizes and nanowire growth time; (d) electrical resistance values when varying the gap sizes and nanowire growth time.

revealed that the structural fusion between opposing two nanostructures significantly occurs at the contact points (Figure S13). In this stage 3, the NO_2 sensing responses significantly decrease. Thus, these *in situ* control experiments of electrical contacts highlight that the sensing characteristics closely correlate to the structural and electrical properties via different electrical contacts between two electrodes. The simplest explanation for this correlation can be given by a necking model between nanostructures for gas sensing.[41,42] Namely, there is an optimum necking size between two ZnO nanowires for NO_2 sensing, which can be tailored by the present *in situ* fabrication method of bridging nanosensors. With the optimum electrical contacts (necking structures) between two nanostructures, stage 2, the electrical current can be significantly modulated by interacting NO_2 molecules on the surface. With thicker necking structures with low electrical resistances, stage 3, the electrical modulation by NO_2 molecules on the surface is rather suppressed because spatially unmodulated electrical conduction paths remain.

Figure 5 shows the application of the proposed methodology to the most conventional interdigitated array electrodes as gas sensors. Figure 5a shows the schematic image of fabricated devices with interdigitated array electrodes (Figures S14 and S15). Figure 5b shows the SEM images of fabricated bridging nanosensors. The gap width of array electrodes and the nanowire length are 2 μm and ~6 μm (8 h growth), respectively. A similar edge-topological regulation effect can be seen in SEM images, as we have seen in Figures 1 and 2. Bridging nanosensors fabricated from edgeless seed layers showed more clear interfaces between two opposing electrodes in top-view SEM images when compared with those fabricated from sharp edge seed layers. Figure 5c shows the comparison between the two bridging nanosensors on the NO_2 sensing behaviors when varying the concentration from 10 ppm down to 5 ppb. The limit of detection (LOD) for bridging nanosensors fabricated from edgeless seed layers is 5 ppb, which is 20 times lower than 100 ppb for bridging nanosensors fabricated from sharp edge seed layers. As discussed in the above section, well-controlled electrical contacts (appropriate

https://doi.org/10.1021/acs.nanolett.1c04600
Nano Lett. 2022, 22, 2569−2577

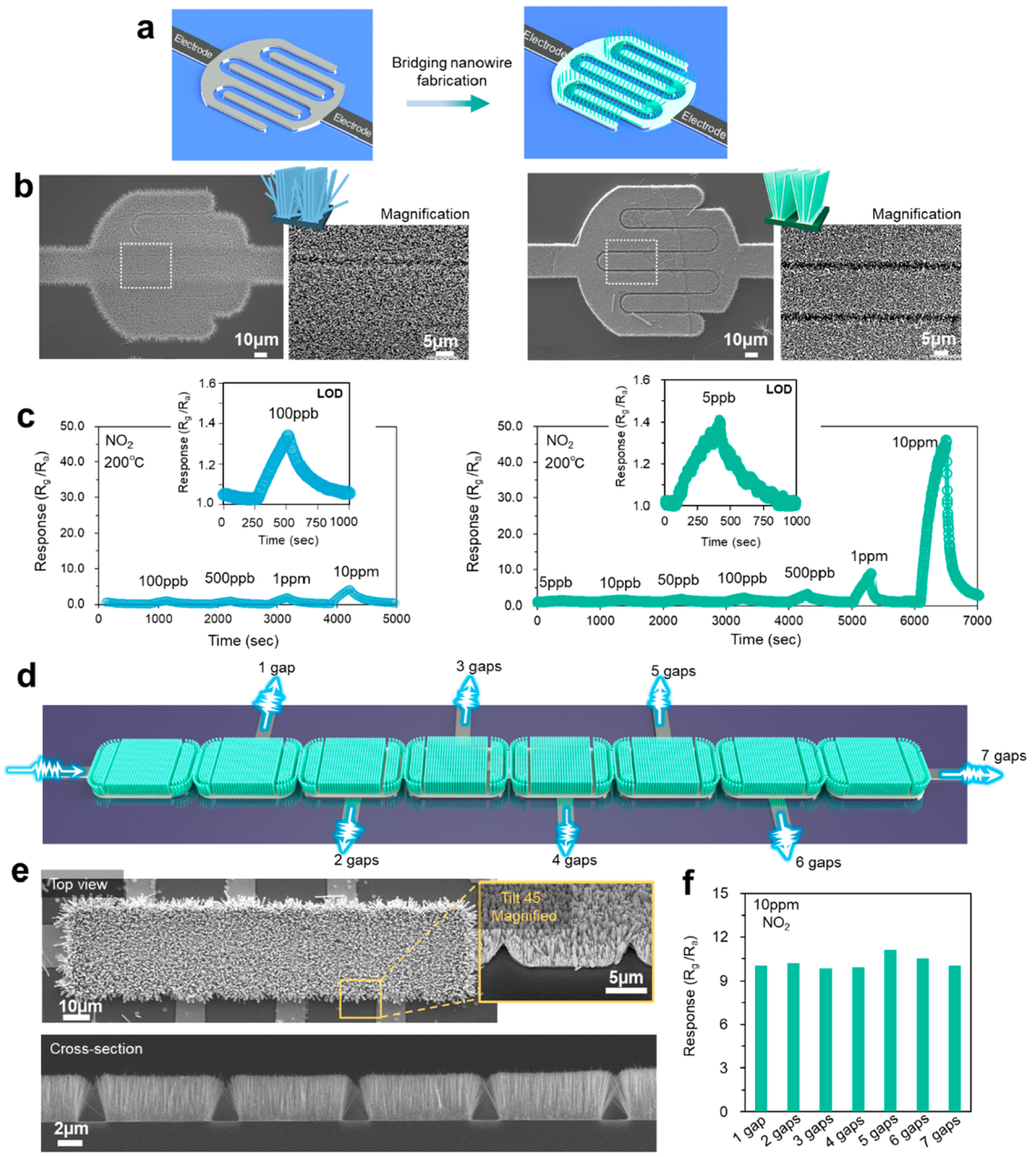

Figure 5. Applicability of present bridging nanosensors to interdigitated array electrodes and integrated multinanosensor arrays: (a) schematic image of fabricated bridging nanosensors with interdigitated array electrodes; (b) comparison between two bridging nanosensors fabricated from the sharp edge seed layer or the edgeless seed layer on SEM images of fabricated bridging nanosensors; (c) comparison between two bridging nanosensors fabricated from the sharp edge seed layer or the edgeless seed layer on NO_2 gas sensing data when varying the concentration; (d) schematic of integrated multibridging nanosensor structure; (e) SEM images of multibridging nanosensor fabricated from an edgeless seed layer (top view, tilt 45° view, and cross-sectional view); (f) NO_2 (10 ppm) sensor responses for fabricated multibridging nanosensor.

necking structures) between two nanostructures are clearly responsible to cause the observed difference between the two bridging nanosensors on the LOD values. Thus, bridging nanosensors fabricated from edgeless seed layers can be applicable to conventional interdigitated array electrodes. Finally, we integrated multibridging nanosensors in series and examined the spatial uniformity of sensing properties toward highly integrated sensor devices, as illustrated in Figure 5d. Figure 5e shows the SEM images of bridging nanosensors fabricated from edgeless seed layers with well-defined microstructures. Figure 5f shows the spatial variation of NO_2 (10 ppm) sensor responses for integrated multibridging nanosensors. Clearly, the sensor response is almost identical and independent of the number of bridging nanosensors in series. In principle, the electrical resistance value in series is dominated by the most resistive junction. If there is a variation of electrical resistances in series, the sensor responses should exhibit a significant junction number dependence. Thus, the insensitivity of junction numbers in series on sensor responses highlights the spatial designability and uniformity of the present method for integrated bridging nanosensor devices on Si substrate.

https://doi.org/10.1021/acs.nanolett.1c04600
Nano Lett. 2022, 22, 2569−2577

CONCLUSION

In summary, we report the significant effect of edge-topological regulation on *in situ* fabrication of ZnO bridging nanosensors. When employing seed layers with a sharp edge, which is a well-defined structure in conventional lithography, the bridging angles and electrical resistances between two opposing electrodes were randomly distributed, and they could not be well controlled. The stochastic nature of bridging growth direction at the sharp edges inherently causes such unintentional variation of structural and electrical properties. We propose an edgeless seed layer structure using two-layers resist methods to solve the above uncontrollability of bridging nanosensors. Bridging nanosensors fabricated using such edgeless seed layer structures not only substantially improved the uniformity of structural and electrical properties between two opposing electrodes but also significantly enhanced the sensing responses for NO_2 with the smaller variance and the lower limit of detection via *in situ* controlled electrical contacts when compared with those using conventional sharp edge seed layers.

EXPERIMENTAL SECTION

Fabrication of Bridging Nanosensors. Bridging nanosensors were fabricated on Si (100) substrates with SiO_2 (100 nm) layer. Photoresist (AZP1350) was employed for conventional lithography to fabricate bridging nanosensors. Spin-coating of photoresists was performed on Si substrates at 4000 rpm for 1 min. Thermal baking procedure was performed at 190 °C for 5 min, and then the patterning process was carried out using a photolithography machine (Heidelberg Instruments μPG 101 UOW1) at an energy of 40 mW. Then, Pt electrode was deposited by radio frequency (RF) sputtering at a power of 50 W and an Ar pressure of 0.3 Pa with the thickness of 100 nm. Subsequently, a Ti thin layer (~5 nm, RF at 50 W) was deposited onto Pt electrodes to enhance the adhesion between ZnO seed layer and electrodes. And then, ZnO seed-layers were deposited on the pattered substrates with the thickness of 50 nm (RF at 50 W). A lift-off process was performed using *N*,*N*-dimethylformamide (DMF). To overcome the sharp-edge issues, we propose a two-layer photoresist method, which employs two laminated resists. Spin-coating positive type photoresist (LOR3B) was performed on Si substrates at 3000 rpm for 1 min. Thermal baking procedure was performed at 100 °C for 2 min. Subsequently, conventional lithography was performed. The gap size of patterned substrates ranged from 2 to10 μm. ZnO bridging nanosensors on patterned seed-layer substrate were formed by a hydrothermal method. The substrate was immersed into a 150 mL aqueous solution containing 25 mM zinc nitrate hexahydrate ($Zn(NO_3)_2{\cdot}6H_2O$, Wako 99.0%) and 25 mM hexamethylenetetramine ($(CH_2)_6N_4$ Wako 99.0%), 2.5 mM polyethylenimine (number-average MW 1800, 50 wt % in H_2O), and ammonia ($NH_3{\cdot}6H_2O$, 1 mL, 28% in H_2O). The ZnO nanowires were grown with keeping the solution at 95 °C in the oven with a constant growth temperature. After the crystal growth, the substrate was taken out from the solution. Twelve devices were fabricated for each condition to obtain statistical data.

Characterization of Bridging Nanosensors. The morphology of fabricated bridging nanosensors was characterized by scanning electron microscopy (SEM, JEOL JSM-7610F) at an accelerating voltage of 15 kV. Electrical properties of bridging nanosensors were measured as *I*−*V* data using a semiconductor parameter analyzer (Keithley, 4200SCS) with a probe station having a temperature-controlling system. Gas sensing measurements were performed using a homemade testing system consisting of a gas supply system, a probe station with temperature control (JANIS, ST-500), and a semiconductor analyzer (Keithley 4200SCS) used to collect the electric signal. The electrical signals under N_2 or NO_2 ppm were measured by applying a voltage of 1 V to the electrodes. The sensor response was defined as R_g/R_a, where R_g and R_a are the sensor resistance when exposed to NO_2 and N_2, respectively. Testing temperature was set to vary from room temperature to 250 °C. Electrical property and gas sensing measurements were controlled under 200 °C.

ASSOCIATED CONTENT

Supporting Information

The Supporting Information is available free of charge at https://pubs.acs.org/doi/10.1021/acs.nanolett.1c04600.

Bridging nanosensors fabricated from sharp edge and edgeless seed layers; electrical properties of bridging nanosensors in air and NO_2 atmosphere; effect of top-view topology on bridging nanosensors; temperature dependent NO_2 sensing property molecular selectivity; effect of sensor length; bridging nanosensors when varying the gap size and the nanowire growth time (PDF)

AUTHOR INFORMATION

Corresponding Author

Takeshi Yanagida − *Department of Applied Chemistry, Graduate School of Engineering, The University of Tokyo, Tokyo 113-8656, Japan; Institute for Materials Chemistry and Engineering, Kyushu University, Kasuga, Fukuoka 816-8580, Japan;* orcid.org/0000-0003-4837-5701; Email: yanagida@g.ecc.u-tokyo.ac.jp

Authors

Jiangyang Liu − *Department of Applied Chemistry, Graduate School of Engineering, The University of Tokyo, Tokyo 113-8656, Japan;* orcid.org/0000-0001-5456-7705

Hao Zeng − *Department of Applied Chemistry, Graduate School of Engineering, The University of Tokyo, Tokyo 113-8656, Japan*

Guozhu Zhang − *Department of Applied Chemistry, Graduate School of Engineering, The University of Tokyo, Tokyo 113-8656, Japan*

Wenjun Li − *Department of Applied Chemistry, Graduate School of Engineering, The University of Tokyo, Tokyo 113-8656, Japan; Institute for Materials Chemistry and Engineering, Kyushu University, Kasuga, Fukuoka 816-8580, Japan*

Kazuki Nagashima − *Department of Applied Chemistry, Graduate School of Engineering, The University of Tokyo, Tokyo 113-8656, Japan; PRESTO, Japan Science and Technology Agency, Kawaguchi-shi, Saitama 332-0012, Japan;* orcid.org/0000-0003-0180-816X

Tsunaki Takahashi − *Department of Applied Chemistry, Graduate School of Engineering, The University of Tokyo, Tokyo 113-8656, Japan; PRESTO, Japan Science and Technology Agency, Kawaguchi-shi, Saitama 332-0012, Japan;* orcid.org/0000-0002-2840-8038

https://doi.org/10.1021/acs.nanolett.1c04600
Nano Lett. 2022, 22, 2569−2577

Takuro Hosomi − *Department of Applied Chemistry, Graduate School of Engineering, The University of Tokyo, Tokyo 113-8656, Japan; PRESTO, Japan Science and Technology Agency, Kawaguchi-shi, Saitama 332-0012, Japan;* orcid.org/0000-0002-5649-6696

Wataru Tanaka − *Department of Applied Chemistry, Graduate School of Engineering, The University of Tokyo, Tokyo 113-8656, Japan*

Masaki Kanai − *Institute for Materials Chemistry and Engineering, Kyushu University, Kasuga, Fukuoka 816-8580, Japan*

Complete contact information is available at: https://pubs.acs.org/10.1021/acs.nanolett.1c04600

Author Contributions

T.Y. designed the experiments and wrotethe manuscript with J.L. Device design and fabrication sensor performance evaluations were performed by J.L., H.Z., and W.L. Morphology characterizations of the bridging nanostructures were conducted by J.L. and H.Z. The gas sensing property analyses were discussed by J.L, H.Z., G.Z., and T.Y. K.N., T.H., M.K., W.T., G.Z., and T.T. contributed to improve the manuscript. All the authors contributed to manuscript preparation and approved the final version of the manuscript.

Notes

The authors declare no competing financial interest.

■ ACKNOWLEDGMENTS

This work was supported by JSPS KAKENHI (Grants JP18H01831, JP18H05243, JP20H02208, JP21K18868, and JP21K14475), CREST (Grant JPMJCR19I2), and AMED (Grant JP21zf0127004). This work was partly performed under the Cooperative Research Program of "Dynamic Alliance for Open Innovation Bridging Human, Environment and Materials" and "Network Joint Research Center for Materials and Devices".

■ REFERENCES

(1) Cai, J.; Ruffieux, P.; Jaafar, R.; Bieri, M.; Braun, T.; Blankenburg, S.; Muoth, M.; Seitsonen, A. P.; Saleh, M.; Feng, X. L.; Mullen, K.; Fasel, R. Atomically Precise Bottom-up Fabrication of Graphene Nanoribbons. *Nature* **2010**, *466*, 470−473.

(2) Zhang, W. X.; Yang, S. H. In Situ Fabrication of Inorganic Nanowire Arrays Grown from and Aligned on Metal Substrates. *Acc. Chem. Res.* **2009**, *42* (10), 1617−1627.

(3) Jensen, J.; Krebs, F. C. From the Bottom up—flexible Solid State Electrochromic Devices. *Adv. Mater.* **2014**, *26* (42), 7231−7234.

(4) Liu, S. T.; Maoz, R.; Sagiv, J. Planned Nanostructures of Colloidal Gold via Self-assembly on Hierarchically Assembled Organic Bilayer Template Patterns with in-situ Generated Terminal Amino Functionality. *Nano Lett.* **2004**, *4* (5), 845−851.

(5) Leicht, P.; Zielke, L.; Bouvron, S.; Moroni, R.; Voloshina, E.; Hammerschmidt, L.; Dedkov, Y. S.; Fonin, M. In Situ Fabrication of Quasi-Free-Standing Epitaxial Graphene Nanoflakes on Gold. *ACS Nano* **2014**, *8* (4), 3735−3742.

(6) Tang, S. Y.; Yang, C. C.; Su, T. Y.; Yang, T. Z.; Wu, S. C.; Hsu, Y. C.; Chen, Y. Z.; Lin, T. Z.; Shen, J. L.; Lin, H. N.; Chiu, P. W.; Kuo, H. C.; Chueh, Y. L. Design of Core−Shell Quantum Dots−3D WS_2 Nanowall Hybrid Nanostructures with High-Performance Bifunctional Sensing Applications. *ACS Nano* **2020**, *14* (10), 12668−12678.

(7) Jiang, H. Chemical Preparation of Graphene-based Nanomaterials and Their Applications in Chemical and Biological Sensors. *Small* **2011**, *7* (17), 2413−2427.

(8) Li, M. W.; Bhiladvala, R. B.; Morrow, T. J.; Sioss, J. A.; Lew, K. K.; Redwing, J. M.; Keating, C. D.; Mayer, T. S. Bottom-up Assembly of Large-area Nanowire Resonator Arrays. *Nat. Nanotechnol.* **2008**, *3* (2), 88−92.

(9) Hawkeye, M. M.; Brett, M. J. Optimized Colorimetric Photonic-crystal Humidity SensorFabricated Using Glancing Angle Deposition. *Adv. Funct. Mater.* **2011**, *21* (19), 3652−3658.

(10) Huang, J. F.; Zhu, Y. H.; Yang, X. L.; Chen, W.; Zhou, Y.; Li, C. Z. Flexible 3D Porous CuO Nanowire Arrays for Enzymeless Glucose Sensing: in situ Engineered Versus ex situ Piled. *Nanoscale* **2015**, *7* (2), 559−569.

(11) Xue, M.; Zhang, Y.; Yang, Y.; Cao, T. Processing Matters: In situ Fabrication of Conducting Polymer Microsensors Enables Ultralow-limit Gas Detection. *Adv. Mater.* **2008**, *20* (11), 2145−2150.

(12) Attia, R.; Pregibon, D. C.; Doyle, P. S.; Viovy, J. L.; Bartolo, D. Soft Microflow Sensors. *Lab Chip* **2009**, *9* (9), 1213−1218.

(13) Gao, W.; Emaminejad, S.; Nyein, H. Y. Y.; Challa, S.; Chen, K.; Peck, A.; Fahad, H. M.; Ota, H.; Shiraki, H.; Kiriya, D.; Lien, D. H.; Brooks, G. A.; Davis, R. W.; Javey, A. Fully Integrated Wearable Sensor Arrays for Multiplexed in situ Perspiration Analysis. *Nature* **2016**, *529* (7587), 509−514.

(14) Mijatovic, D.; Eijkel, J. C. T.; Van den Berg, A. Technologies for Nanofluidic Systems: top-down vs. bottom-up—a review. *Lab Chip* **2005**, *5* (5), 492−500.

(15) Yang, P. D.; Yan, R. X.; Fardy, M. Semiconductor Nanowire: What's next? *Nano Lett.* **2010**, *10* (5), 1529−1536.

(16) Mehta, R. J.; Zhang, Y. L.; Karthik, C.; Singh, B.; Siegel, R. W.; Borca-Tasciuc, T.; Ramanath, G. A New Class of Doped Nanobulk High-Figure-of-Merit Thermoelectrics by Scalable Bottom-up Assembly. *Nat. Mater.* **2012**, *11* (3), 233−240.

(17) Zhao, D.; Huang, H.; Chen, S.; Li, Z.; Li, S.; Wang, M.; Zhu, H.; Chen, X. In situ Growth of Leakage-Free Direct-Bridging GaN Nanowires: Application to Gas Sensors for Long-Term Stability, Low Power Consumption, and Sub-ppb Detection Limit. *Nano Lett.* **2019**, *19* (6), 3448−3456.

(18) Steinhauer, S.; Chapelle, A.; Menini, P.; Sowwan, M. Local CuO Nanowire Growth on Microhotplates: In situ Electrical Measurements and Gas Sensing Application. *ACS Sensors* **2016**, *1* (5), 503−507.

(19) Park, W. J.; Choi, K. J.; Kim, M. H.; Koo, B. H.; Lee, J. L.; Baik, J. M. Self-Assembled and Highly Selective Sensors Based on Air-Bridge-Structured Nanowire Junction Arrays. *ACS Appl. Mater. Interfaces* **2013**, *5* (15), 6802−6807.

(20) Han, H.; Kim, J.; Shin, H. S.; Song, J. Y.; Lee, W. Air-Bridged Ohmic Contact on Vertically Aligned Si Nanowire Arrays: Application to Molecule Sensors. *Adv. Mater.* **2012**, *24* (17), 2284−2288.

(21) Qi, P.; Vermesh, O.; Grecu, M.; Javey, A.; Wang, Q.; Dai, H.; Peng, S.; Cho, K. J. Toward Large Arrays of Multiplex Functionalized Carbon Nanotube Sensors for Highly Sensitive and Selective Molecular Detection. *Nano Lett.* **2003**, *3* (3), 347−51.

(22) Kamins, T. I.; Sharma, S.; Yasseri, A. A.; Li, Z.; Straznicky, J. Metal-catalysed, Bridging Nanowires as Vapour Sensors and Concept for their Use in a Sensor System. *Nanotechnology* **2006**, *17* (11), S291.

(23) Ahn, M. W.; Park, K. S.; Heo, J. H.; Park, J. G.; Kim, D. W.; Choi, K. J.; Lee, J. H.; Hong, S. H. Gas Sensing Properties of Defect-controlled ZnO-nanowire Gas Sensor. *Appl. Phys. Lett.* **2008**, *93* (26), 263103.

(24) Woo, H. S.; Kwak, C. H.; Kim, I. D.; Lee, J. H. Selective, Sensitive, and Reversible Detection of H_2S Using Mo-doped ZnO Nanowire Network Sensors. *Journal of Materials Chemistry A* **2014**, *2* (18), 6412−6418.

(25) Thong, L. V.; Hoa, N. D.; Le, D. T. T.; Viet, D. T.; Tam, P. D.; Le, A.-T.; Hieu, N. V. On-chip Fabrication of SnO_2-nanowire Gas Sensor: The Effect of Growth Time on Sensor Performance. *Sens. Actuators, B* **2010**, *146* (1), 361−367.

(26) Steinhauer, S.; Chapelle, A.; Menini, P.; Sowwan, M. Local CuO Nanowire Growth on Microhotplates: In Situ Electrical

Measurements and Gas Sensing Application. *ACS Sensors* **2016**, *1* (5), 503−507.
(27) Zhao, D.; Huang, H.; Chen, S.; Li, Z.; Li, S.; Wang, M.; Zhu, H.; Chen, X. In Situ Growth of Leakage-free Direct-bridging GaN Nanowires: Application to Gas Sensors for Long-term Stability, Low Power Consumption, and Sub-ppb Detection Limit. *Nano Lett.* **2019**, *19* (6), 3448−3456.
(28) Offermans, P.; Crego-Calama, M.; Brongersma, S. H. Gas Detection with Vertical InAs Nanowire Arrays. *Nano Lett.* **2010**, *10* (7), 2412−2415.
(29) Pan, X.; Liu, X.; Bermak, A.; Fan, Z. Self-gating Effect Induced Large Performance Improvement of ZnO Nanocomb Gas Sensors. *ACS Nano* **2013**, *7* (10), 9318−9324.
(30) Fan, Z.; Wang, D.; Chang, P. C.; Tseng, W. Y.; Lu, J. G. ZnO Nanowire Field-effect Transistor and Oxygen Sensing Property. *Appl. Phys. Lett.* **2004**, *85* (24), 5923−5925.
(31) Liu, J.; Nagashima, K.; Yamashita, H.; Mizukami, W.; Uzuhashi, J.; Hosomi, T.; Kanai, M.; Zhao, X.; Miura, Y.; Zhang, G.; Takahashi, T.; Suzuki, M.; Sakai, D.; Samransuksamer, B.; He, Y.; Ohkubo, T.; Yasui, T.; Aoki, Y.; Ho, J. C.; Baba, Y.; Yanagida, T. Face-selective Tungstate Ions Drive Zinc Oxide Nanowire Growth Direction and Dopant Incorporation. *Communications Materials* **2020**, *1* (1), 1−10.
(32) Wang, C.; Hosomi, T.; Nagashima, K.; Takahashi, T.; Zhang, G.; Kanai, M.; Zeng, H.; Mizukami, W.; Shioya, N.; Shimoaka, T.; Tamaoka, T.; Yoshida, H.; Takeda, S.; Yasui, T.; Baba, Y.; Aoki, Y.; Terao, J.; Hasegawa, T.; Yanagida, T. Rational Method of Monitoring Molecular Transformations on Metal-oxide Nanowire Surfaces. *Nano Lett.* **2019**, *19* (4), 2443−2449.
(33) Joo, J.; Chow, B. Y.; Prakash, M.; Boyden, E. S.; Jacobson, M. Face-selective Electrostatic Control of Hydrothermal Zinc Oxide Nanowire Synthesis. *Nat. Mater.* **2011**, *10* (8), 596−601.
(34) He, Y.; Yanagida, T.; Nagashima, K.; Zhuge, F.; Meng, G.; Xu, B.; Klamchuen, A.; Rahong, S.; Kanai, M.; Li, X.; Suzuki, M.; Kai, S.; Kawai, T. Crystal-plane Dependence of Critical Concentration for Nucleation on Hydrothermal ZnO Nanowires. *J. Phys. Chem. C* **2013**, *117* (2), 1197−1203.
(35) Chen, L. Y.; Yin, Y. T.; Chen, C. H.; Chiou, J. Influence of Polyethyleneimine and Ammonium on the Growth of ZnO Nanowires by Hydrothermal Method. *J. Phys. Chem. C* **2011**, *115* (43), 20913−20919.
(36) Greene, L. E.; Law, M.; Tan, D. H.; Montano, M.; Goldberger, J.; Somorjai, G.; Yang, P. General Route to Vertical ZnO Nanowire Arrays Using Textured ZnO Seeds. *Nano Lett.* **2005**, *5* (7), 1231−1236.
(37) Guillemin, S.; Consonni, V.; Appert, E.; Puyoo, E.; Rapenne, L.; Roussel, H. Critical Nucleation Effects on the Structural Relationship Between ZnO Seed Layer and Nanowires. *J. Phys. Chem. C* **2012**, *116* (47), 25106−25111.
(38) Lao, J. Y.; Huang, J. Y.; Wang, D. Z.; Ren, Z. F. ZnO Nanobridges and Nanonails. *Nano Lett.* **2003**, *3* (2), 235−238.
(39) Zhao, C. X.; Li, Y. F.; Zhou, J.; Li, L.; Deng, S. Z.; Xu, N. S.; Chen, J. Large-scale Synthesis of Bicrystalline ZnO Nanowire Arrays by Thermal Oxidation of Zinc Film: Growth Mechanism and High-performance Field Emission. *Cryst. Growth Des.* **2013**, *13* (7), 2897−2905.
(40) Yang, P.; Yan, H.; Mao, S.; Russo, R.; Johnson, J.; Saykally, R.; Morris, N.; Pham, J.; He, R.; Choi, H. J. Controlled Growth of ZnO Nanowires and Their Optical Properties. *Adv. Funct. Mater.* **2002**, *12* (5), 323−331.
(41) Scott, R. W.; Yang, S. M.; Coombs, N.; Ozin, G. A.; Williams, D. E. Engineered Sensitivity of Structured Tin Dioxide Chemical Sensors: Opaline Architectures with Controlled Necking. *Adv. Funct. Mater.* **2003**, *13* (3), 225−231.
(42) Jun, J. H.; Yun, J.; Cho, K.; Hwang, I. S.; Lee, J. H.; Kim, S. Necked ZnO Nanoparticle-based NO_2 Sensors with High and Fast Response. *Sens. Actuators, B* **2009**, *140* (2), 412−417.

https://doi.org/10.1021/acs.nanolett.1c04600
Nano Lett. 2022, 22, 2569−2577